

# Unintended Effects on Adaptive Learning Rate for Training Neural Network with Output Scale Change

Ryuichi Kanoh<sup>1,2</sup> Mahito Sugiyama<sup>1,2,3</sup>

## Abstract

A multiplicative constant scaling factor is often applied to the model output to adjust the dynamics of neural network parameters. This has been used as one of the key interventions in an empirical study of lazy and active behavior. However, we show that the combination of such scaling and a commonly used adaptive learning rate optimizer strongly affects the training behavior of the neural network. This is problematic as it can cause *unintended behavior* of neural networks, resulting in the misinterpretation of experimental results. Specifically, for some scaling settings, the effect of the adaptive learning rate disappears or is strongly influenced by the scaling factor. To avoid the unintended effect, we present a modification of an optimization algorithm and demonstrate remarkable differences between adaptive learning rate optimization and simple gradient descent, especially with a small ( $< 1.0$ ) scaling factor.

## 1. Introduction

Deep learning (LeCun et al., 2015) has penetrated machine learning and data analytics, and is used in a variety of applications. However, its behavior is not well understood. In recent years, various insights have been gained by linearly approximating the training of neural networks. One of the most common tools used with a linear approximation is *Neural Tangent Kernel* (NTK) (Jacot et al., 2018):

$$\Theta(\theta, x_1, x_2) = \nabla_\theta f(\theta, x_1) \nabla_\theta f(\theta, x_2), \quad (1)$$

where  $x_1, x_2$  are two inputs to the model, and  $\nabla_\theta f$  is the gradient of the model output  $f$  with respect to the model parameters  $\theta$ . If the change of  $\Theta$  during training is negligible, implying a small parameter change during training, NTK becomes a vital tool for explaining the good trainability and

<sup>1</sup>National Institute of Informatics <sup>2</sup>The Graduate University for Advanced Studies, SOKENDAI <sup>3</sup>JST, PRESTO. Correspondence to: Ryuichi Kanoh <kanoh@nii.ac.jp>.

Preliminary work.

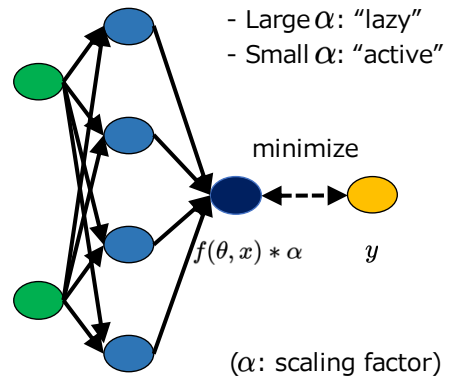


Figure 1. Schematics on output scaling.

generalization performance of neural networks (Allen-Zhu et al., 2019; Du et al., 2019b; Arora et al., 2019; Lee et al., 2019). However, the linear approximation, or the frozen  $\Theta$  assumption, may not work for realistic neural network models (Ghorbani et al., 2019). Therefore, a number of studies (Chizat et al., 2019; D'Ascoli et al., 2020; Geiger et al., 2020b;a; Woodworth et al., 2020) have emerged to investigate the difference in behavior between lazy regimes and active regimes. Here, a *lazy regime* is a regime in which the change in parameters is small relative to the initial value, and a linear approximation is reasonable. In contrast, an *active regime* is a regime in which the change in parameters is not small, and a linear approximation is no longer valid.

To empirically compare the behavior of the lazy regime and active regime, Chizat et al. (2019) introduced a useful method, which multiplies the output of the neural network by a positive constant scaling factor  $\alpha$ ,

$$F(\theta, x) = \alpha f(\theta, x), \quad (2)$$

where  $f$  and  $F$  are the original and scaled output of a neural network, respectively (Figure 1). If the scaling factor  $\alpha$  is large, even small changes in model parameters can significantly change the output, so the behavior approaches laziness. In contrast, if  $\alpha$  is close to zero, the amount of parameter change is relatively large, and the behavior becomes active. Using these properties, Chizat et al. (2019) conducted an empirical study using image recognition mod-

els such as ResNet (He et al., 2016) and VGG (Simonyan & Zisserman, 2015), and showed that lazy training does not perform well. It implies that understanding practical neural networks' success requires an understanding outside the framework of linear approximation. As a result, analyses beyond linear approximation are becoming more widespread (Li et al., 2020; Bai & Lee, 2020). For instance, the *mean-field* (MF) theory is used (Mei et al., 2018; Chizat & Bach, 2018) to describe training dynamics of the neural network without the laziness assumption. Compared to the NTK theory, the values multiplied by the final layer scaling are set to be smaller in the MF theory, resulting in more active behavior.

It should be noted that, while there are a number of examples that demonstrate the importance of active behavior as we described above, it does not necessarily mean that lazy behavior does not benefit. For example, Geiger et al. (2020b) and Lee et al. (2020) showed that the appropriate regime depends on the dataset and neural network architecture, and that lazy training often outperforms active training on fully connected neural networks. Arora et al. (2020) showed that the model trained using the NTK, taking over lazy training, performs better than the standard neural network model on UCI datasets. Du et al. (2019a) evaluated training time and showed that there are cases in which the training with NTK performs better and faster than the algorithm with standard backpropagation. These results indicate that lazy training potentially has not only theoretical but also practical advantages. Therefore, in real-world applications, the scaling factor can be considered as a hyper-parameter for determining behavior, like the learning rate and the neural network model's structure. Understanding of lazy training via the scaling factor has become an exciting research topic from both theoretical and practical viewpoints.

In this paper, we show that the combination of *output scaling* and an *adaptive learning rate optimizer* strongly affects the neural network training behavior, which leads to misinterpretation of empirical investigation. An adaptive learning rate optimizer, such as *adaptive moment estimation* (Adam) (Kingma & Ba, 2015) or *root mean square propagation* (RMSProp) (Tieleman & Hinton, 2012), are often used to achieve fast and stable behavior (D'Ascoli et al., 2020; Geiger et al., 2020b). We demonstrate that such optimizers induce unintended behavior as the optimization algorithm strongly influences the parameter dynamics. To counteract unintended effects, we propose a modification of the optimization algorithm and show that it can properly adjust for unintended effects. With this modification, we can properly compare the behavior with simple gradient descent. In our numerical experiment, using the modified optimizer, we observe the behavioral difference between simple gradient descent and adaptive learning rate optimizer.

We summarize our contribution in the following.

1. We point out that the combination of scaling and adaptive learning rate optimizer causes unintended behavior, which induces a misinterpretation of empirical investigations. This may change results of some previous studies.
2. To solve the problem, we propose to modify the optimization algorithm and show that it can properly adjust for unintended effects.
3. Using the modified optimizer, we observe the behavioral difference between simple gradient descent and an adaptive learning rate optimizer. Especially, under the setting of the scaling factor  $\alpha < 1.0$  and hyper-parameters that give accurate classification:
  - (a) The range of hyper-parameters with the adaptive learning rate optimizer is wider than that with the simple gradient descent, implying higher robustness to hyper-parameter selection.
  - (b) The power law that hyper-parameters follow is different between the simple gradient descent and the adaptive learning rate optimizer. For the same scaling factor, the proper learning rate with the adaptive learning rate optimizer becomes larger than that with the simple gradient descent.
  - (c) For the adaptive learning rate optimizer, consistency of hidden features during the training is likely to be smaller than that of the simple gradient descent.

## 2. Unintended effects induced by scaling and adaptive learning rate

The objective of training neural networks is to minimize the following error function:

$$\mathcal{L}(\theta) = \frac{1}{n} \sum_{(x,y) \in \mathcal{T}} \ell(f(\theta, x), y), \quad (3)$$

where  $\ell$  is the loss per sample with a ground truth label  $y$ ,  $\mathcal{T}$  is a training dataset with size  $n$ . The loss function introduced in (Chizat et al., 2019) for experiments with an output scaling factor is given as

$$\mathcal{L}(\theta) = \frac{1}{\alpha^2 n} \sum_{(x,y) \in \mathcal{T}} \ell\left(\alpha(f(\theta, x) - f(\theta_0, x)), y\right), \quad (4)$$

where  $\theta_0$  is a model parameter at initialization. Compared to the standard loss function shown in Equation (3), there are two differences. First, it forces the model's output to be zero at the start of training by subtracting the initial prediction value. This modification prevents an immense loss value at

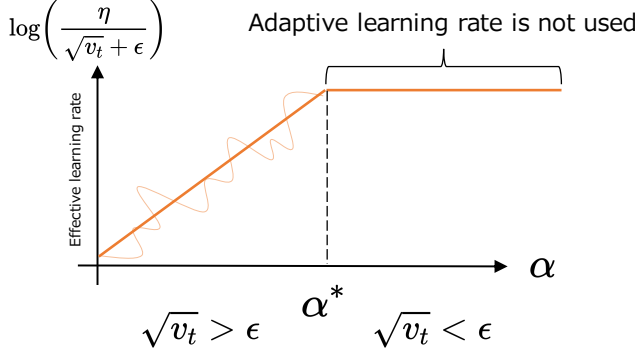


Figure 2. Effective learning rate dependency on the scaling factor with original RMSProp. The wavy line indicates the range in which the adaptive learning rate is properly used. In this case, effect on adaptive learning rate disappear with  $\alpha > \alpha^*$ . Further, even with  $\alpha < \alpha^*$ , effective learning rate depends on  $\alpha$ , that is not desirable for comparison.

the beginning of the training period when  $\alpha \gg 1$ . Second, not only the model output scaling with  $\alpha$  but also the loss function is scaled by  $\alpha^{-2}$ . With loss scaling by  $\alpha^{-2}$ , a comparison with different scaling factors is valid because of

$$\alpha \dot{f}(\theta, x) = \alpha \nabla_{\theta} f(\theta, x) \dot{\theta} \sim \mathcal{O}(\alpha^0), \quad (5)$$

where the  $\dot{f}$  and  $\dot{\theta}$  are time-derivative of  $f$  and  $\theta$ , and a notation  $\mathcal{O}$  is the Bachmann–Landau notation.

As for an optimization algorithm, simple gradient descent is formulated as follows:

$$\theta_{t+1} = \theta_t - \eta G_t, \quad (6)$$

where  $\eta$  and  $G_t$  are a learning rate and the gradient of the loss function (e.g., Equation (3) and (4)) at the  $t$ -th step, respectively.

Looking at an adaptive learning rate procedure, the algorithm for parameter update used in RMSProp (Tieleman & Hinton, 2012) is given as

$$\theta_{t+1} = \theta_t - \frac{\eta}{\sqrt{v_t} + \epsilon} G_t, \quad (7)$$

where

$$v_t = \rho v_{t-1} + (1 - \rho) G_t^2, \quad (8)$$

$\epsilon$  is a small scalar value for preventing zero division, and  $\rho$  is a decay rate for the weight of recent gradient values. RMSProp is a special case of Adam (Kingma & Ba, 2015), with the only difference being that there is no momentum term.

Here we show that combining scaling (Equation (4)) and an adaptive learning rate algorithm (Equation (7) and (8)) induces *unintended effects*, while this combination has been already used in some studies (e.g., D’Ascoli et al. (2020);

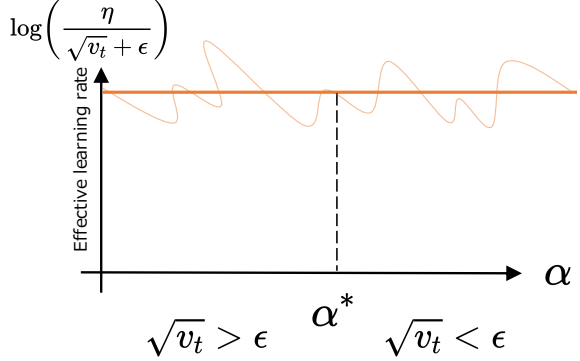


Figure 3. Effective learning rate dependency on the scaling factor with modified RMSProp. The wavy line indicates the range in which the adaptive learning rate is properly used. In this case, the adaptive learning rate’s effect does not disappear with  $\alpha > \alpha^*$  and the effective learning rate does not depend on  $\alpha$  anywhere.

Geiger et al. (2020b)). Figure 2 is the schematic image of the effective learning rate dependency on  $\alpha$ . The key observation is that the value of  $v_t$  in Equation (8), which is used to adaptively determine the effective learning rate in RMSProp, depends on  $\alpha$  as

$$v_t \sim \mathcal{O}(\alpha^{-2}), \quad (9)$$

due to the fact that

$$G_t = \alpha^{-2} \nabla_{\theta} \mathcal{L}(\alpha f(\theta, x)) \sim \mathcal{O}(\alpha^{-1}). \quad (10)$$

Since  $\epsilon$  in Equation (7) does not depend on  $\alpha$ , there is a critical value  $\alpha^*$ , where  $\sqrt{v_t} = \epsilon$ . If  $\alpha$  is sufficiently larger than  $\alpha^*$ , the effect of  $v_t$  becomes smaller, and the impact of  $\alpha$  on the adaptive learning rate becomes almost negligible. However, if  $\alpha$  is smaller than  $\alpha^*$ , the effect of the adaptive learning rate is present, and the effective learning rate  $\eta/(\sqrt{v_t} + \epsilon)$  of RMSProp depends on  $\alpha$ . Therefore, *the effect of the output scaling and the effective learning rate change cannot be disentangled*. Because of this entanglement, we need to update the optimization algorithm to disentangle the effects on change of the scaling factor and the effective learning rate.

We present our proposal of the modified RMSProp optimizer in Algorithm 1, which modifies RMSProp to cancel an unintended effect and achieve the disentanglement. Figure 3 is the schematic image of the effective learning rate dependency on  $\alpha$  with the proposed optimizer. The difference to Equation (8) is that the gradient term  $G_t$  used to compute  $v_t$  is  $\alpha$ -folded as,

$$v_t = \rho v_{t-1} + (1 - \rho)(\alpha G_t)^2. \quad (11)$$

It makes  $v_t$  independent of  $\alpha$  as  $G_t \sim \mathcal{O}(\alpha^{-1})$ , and the effective learning rate no longer depends on  $\alpha$ . Algorithm 1 is a generalization of the conventional RMSProp and is

---

**Algorithm 1** Modified RMSProp optimizer for eliminating scaling factor dependency on learning rate

---

```

input :  $\theta_0, x$ 
initialize :  $v_0 \leftarrow 0, t \leftarrow 0$ 
while  $\theta_t$  does not converge do
     $G_t \leftarrow \frac{1}{\alpha^2} \nabla_{\theta} \mathcal{L}(\alpha(f(\theta_t, x) - f(\theta_0, x)))$ 
     $v_t \leftarrow \rho v_t + (1 - \rho)(\alpha G_t)^2$  (Compared with the original RMSProp,  $G_t$  is  $\alpha$ -folded)
     $\theta_t \leftarrow \theta_t - \frac{\eta}{\sqrt{v_t + \epsilon}} G_t$ 
     $t \leftarrow t + 1$ 
end
output :  $\theta_t$ 

```

---

consistent with the unmodified behavior when  $\alpha = 1$ . This modification can be applied not only to RMSProp but also to other optimization methods such as Adam that has the same elements.

### 3. Setup on numerical experiments

We conduct numerical experiments with a two-layer neural network using the modified optimizer in Algorithm 1. With reference to a similar work, procedures for experiments are based on Geiger et al. (2020b).

**Model architecture** A Two-layer neural network is used for numerical experiments, which is defined as

$$\hat{z} = d^{-1/2} W^0 x, \quad (12)$$

$$z = \sigma(\hat{z}), \quad (13)$$

$$f(\theta, x) = h^{-1/2} W^1 z, \quad (14)$$

where  $d \in \mathbb{N}$  is the size of an input vector, and  $h \in \mathbb{N}$  is the width of the intermediate layer of the neural network (1,000 in numerical experiments). All the weights  $W^0 \in \mathbb{R}$ ,  $W^1 \in \mathbb{R}$  are initialized as standard Gaussian random variables,  $W^1, W^2 \sim \mathcal{N}(0, 1)$ . The bias parameter is not used for simplicity. The scaled softplus function  $\frac{a}{\beta} \ln(1 + e^{\beta x})$  is used for activation function  $\sigma$ , where  $a$  is determined by Monte Carlo method to ensure that the variance of preactivation is 1.  $\beta$  is set it to be 5.

**Dataset** The MNIST (LeCun & Cortes, 2010), Fashion-MNIST (Xiao et al., 2017) and CIFAR10 (Krizhevsky et al.) dataset are used for numerical experiments. Two-dimensional data were converted to a one-dimensional vector (length  $d \in \mathbb{N}$ ) and used as input to a fully connected neural network. Here, to speed up the experiment, the training dataset is randomly subsampled up to 10,000 (20% of the datasets). The dataset for evaluation is not subsampled from the original dataset size (10,000 in total). The input is normalized to be on the sphere  $\sum_i x_i^2 = d$ .

**Loss function** We use soft hinge loss,

$$\ell(f(\theta, x), y) = \frac{1}{\beta} \ln(1 + e^{\beta(1 - f(\theta, x)y)}), \quad (15)$$

for the 10 class classification task, where  $y = \pm 1$  for positive and negative labels for each class, respectively.  $\beta = 20$  for soft hinge loss. As described in Section 2, loss scaling and initial prediction shift are used for calculating the loss value.

**Optimization** The hyper-parameters of RMSProp,  $\rho$  and  $\epsilon$  (see Equation 7, 8), are set to 0.999 and  $10^{-8}$ , respectively. These values are used for both the modified and unmodified algorithms.  $v_0$  is set to be 0. We perform  $5 \times 10^3$  full-batch gradient descent steps with the simple gradient descent, RMSProp, and modified RMSProp optimizer. Double precision is used for all calculations. Note that there are some cases where this precision is not sufficient, depending on the setting of  $\eta$  and  $\alpha$  (Details in Section 4).

**Metric** We report top-1 accuracy on the evaluation dataset. Performances for training dataset is in Supplementary material. We also report a consistency of the hidden features  $\hat{z}$  obtained with initial and trained neural network models for evaluating the degree of the dynamics of parameters. Specifically, consistency is the percentage of hidden features on each neuron that have the same sign before and after training.

## 4. Result and Discussion

### 4.1. Impacts on the Algorithm Modification

Figures 4, 5, and 6 show classification accuracy on the different datasets with a variety of  $\eta$  and  $\alpha$ , where a significant difference is observed between the modified and the original RMSProp. On the right-hand side of each plot, implying  $\alpha > \alpha^*$ , the positive trend observed in  $\alpha$  and  $\eta$  is similar to that of the simple gradient descent and the original RMSProp. While on the left-hand side of each plot, implying  $\alpha < \alpha^*$ , the characteristic slope of the original RMSProp is

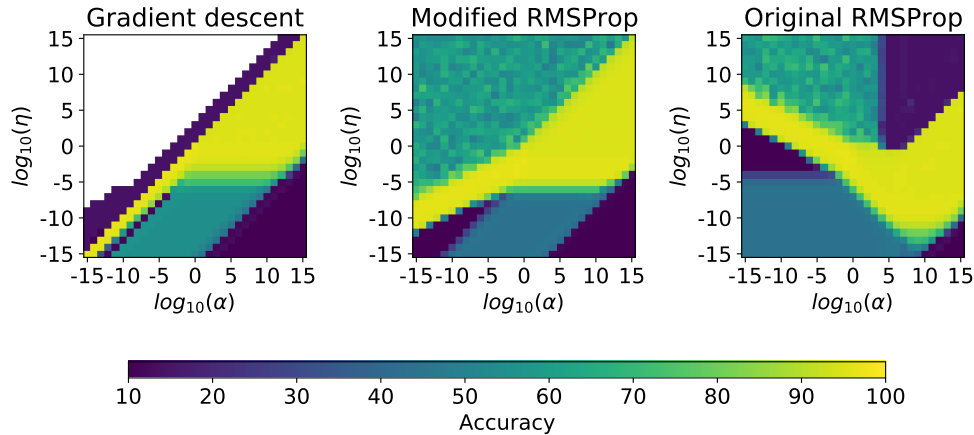


Figure 4. Two-dimensional plots of classification accuracy on the MNIST evaluation dataset. The white area in the figure of gradient descent represents the divergence of training errors.

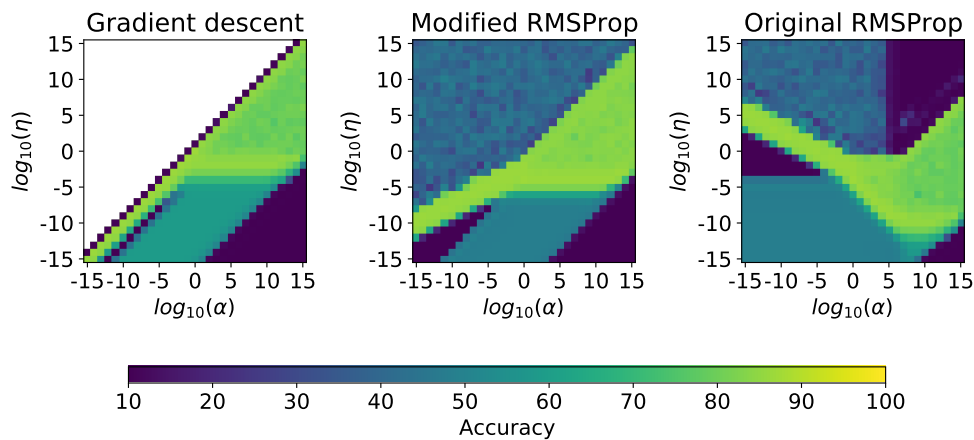


Figure 5. Two-dimensional plots of classification accuracy on the Fashion-MNIST evaluation dataset. The white area in the figure of gradient descent represents the divergence of training errors.

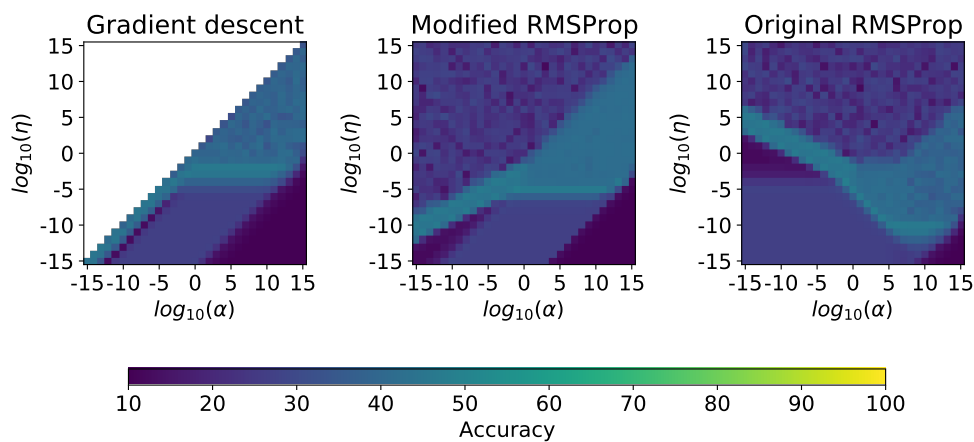


Figure 6. Two-dimensional plots of classification accuracy on the CIFAR-10 evaluation dataset. The white area in the figure of gradient descent represents the divergence of training errors.

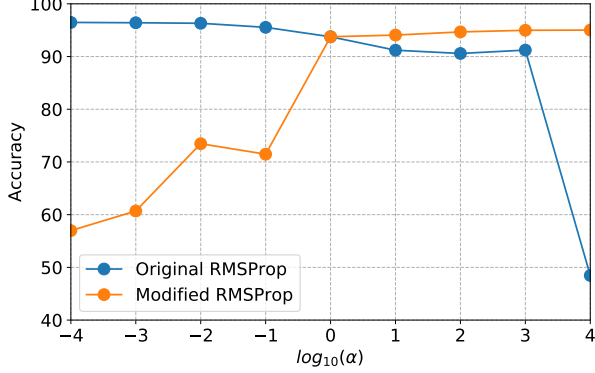


Figure 7. Classification accuracy on the MNIST dataset with  $\eta = 1.0$ . In the case of original RMSProp, the performance is better when  $\alpha$  is small, implying active training. On the other hand, in modified RMSProp, the performance is better when  $\alpha$  is large, implying lazy training.

bent around 90 degrees compared to the modified RMSProp. These observations are consistent with the explanation of the change in the effective learning rate with  $\alpha$ , described in Section 2. It means that our proposed method succeeds in erasing the dependence of effective learning rate on  $\alpha$  as intended. We find that the trend does not change significantly as the dataset changes.

The positive trend observed in Figures 4, 5, and 6 in  $\alpha$  and  $\eta$  for simple gradient descent and modified RMSProp can be understood by considering the impact of  $\alpha$  on the Hessian. It is known that there is a necessary condition of the learning rate and the eigenvalue of the Hessian for the simple gradient descent training convergence (LeCun et al., 1998; 1993),  $\eta < 2/\lambda_{\max}$ , where  $\lambda_{\max}$  is the maximum eigenvalue of the Hessian. Since model output is scaled by  $\alpha$ , its corresponding hessian  $\nabla_{\theta_i} \nabla_{\theta_j} \alpha f(\theta, x)$  is also scaled by  $\alpha$ . Further, since the loss is scaled by  $\alpha^{-2}$  (Equation (4)) in our experiment, the proper  $\eta$  for training that are roughly proportional to  $\eta < 2/\lambda_{\max}$  is scaled by  $\mathcal{O}(\alpha^1)$ . Therefore, there is a positive trend between  $\alpha$  and  $\eta$ .

Note that performance becomes worse in the region of small  $\eta$  and large  $\alpha$  because of the lack of numerical precision in computation. Under such a situation, parameter change,  $\eta G_t$ , becomes relatively small compared to the model parameter  $\theta$ . Because of that, we observe a completely unchanged  $\theta$  from initialization in our numerical experiments. Therefore, experiments with such extreme settings should not be trusted.

Figure 7 illustrates the classification accuracy with respect to the changes of the scaling factor  $\alpha$  of RMSProp with  $\eta = 1.0$  fixed before and after modification. The range of  $\alpha$  is from  $10^{-4}$  to  $10^4$  to guarantee sufficient computational precision with  $\eta = 1.0$ . As the figure shows, before and af-

ter the modification, the conclusions entirely switch, that is, a larger  $\alpha$  (lazy regime) is better for the modified RMSProp and a smaller  $\alpha$  (active regime) is better for the original RMSProp. This observation implies that our modification (Algorithm 1) is crucial in the evaluation of the scaling factor. Additionally, this kind of experimental protocols, which examines performance by changing  $\alpha$ , has been commonly used in previous studies. Therefore, part of the empirical results (Geiger et al., 2020b; D’Ascoli et al., 2020) may be affected by these unintended effects.

## 4.2. Comparison to the simple gradient descent

The comparison between the modified RMSProp and a simple gradient descent provides some interesting behavioral changes. Significant differences are often observed when  $\alpha$  is small, implying active training.

### 4.2.1. PERFORMANCE ROBUSTNESS

When we use an adaptive learning rate optimizer with a small  $\alpha$ , Figures 4, 5, and 6 show that there is a wide range of  $\eta$  values to achieve high-performance ( $\sim 100\%$  accuracy) when compared with a simple gradient descent. This implies the effects on the robustness of the performance to the choice of hyper-parameters, and maybe an example of the remarkable effect of the adaptive learning rate.

### 4.2.2. PROPER HYPER-PARAMETER SETTING

With the modified RMSProp, the characteristic slope is folded around  $\log_{10} \alpha \sim -2$  in Figures 4, 5, and 6. Such folding is not observed with a simple gradient descent case. Because of this behavior, when we use an adaptive learning rate optimizer with a small  $\alpha$ , the value of an appropriate  $\eta$  is likely to be larger than that with a simple gradient descent. Although the reason for such folding is not clear so far, the effect may be due to the switching of inductive biases tied to changes in scaling (Chizat & Bach, 2020). For example, the so-called NTK-regime and MF-regime are known to transition between an output scaling of  $1/\sqrt{h}$  and  $1/h$  (Jacot et al., 2018; Mei et al., 2018), where  $h$  is the width of the hidden layer of the model, and these values are similar to where the observed trend transitions occur. Note that 1,000 is used for  $h$  in our numerical experiments (Section 3).

### 4.2.3. HIDDEN FEATURE CONSISTENCY

Figure 8 shows the hidden feature consistency introduced in Section 3. Figure 9 shows the three dimensional plot that combines Figures 4 and 8. For both simple gradient descent and the modified RMSProp, we can see that the classification accuracy is high in the region where the  $\eta$  and  $\alpha$  are both small. In addition, the sign consistency of hidden features is small in these regions, indicating that

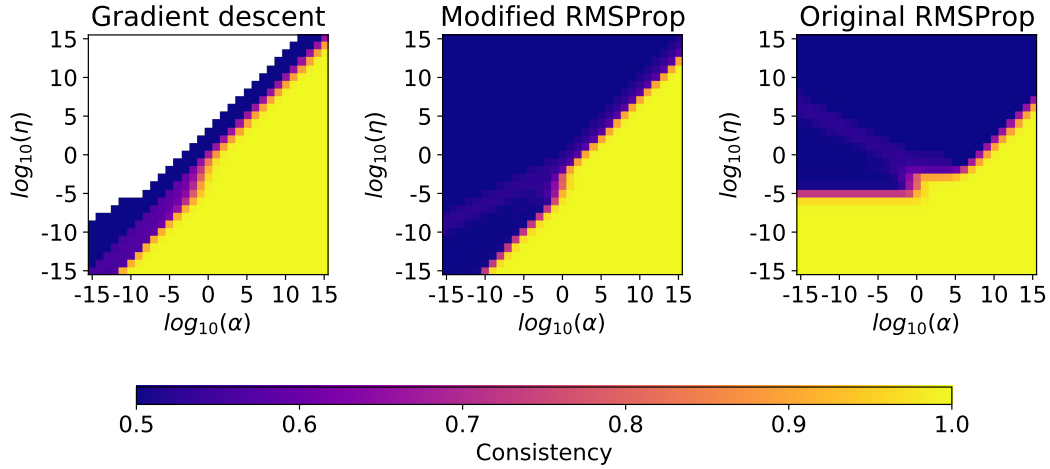


Figure 8. Consistency of the hidden feature signs ( $\pm$  of  $\hat{z}$  for each neuron) obtained with initial and trained neural network models. Hidden features are extracted by use of the evaluation dataset of the MNIST.

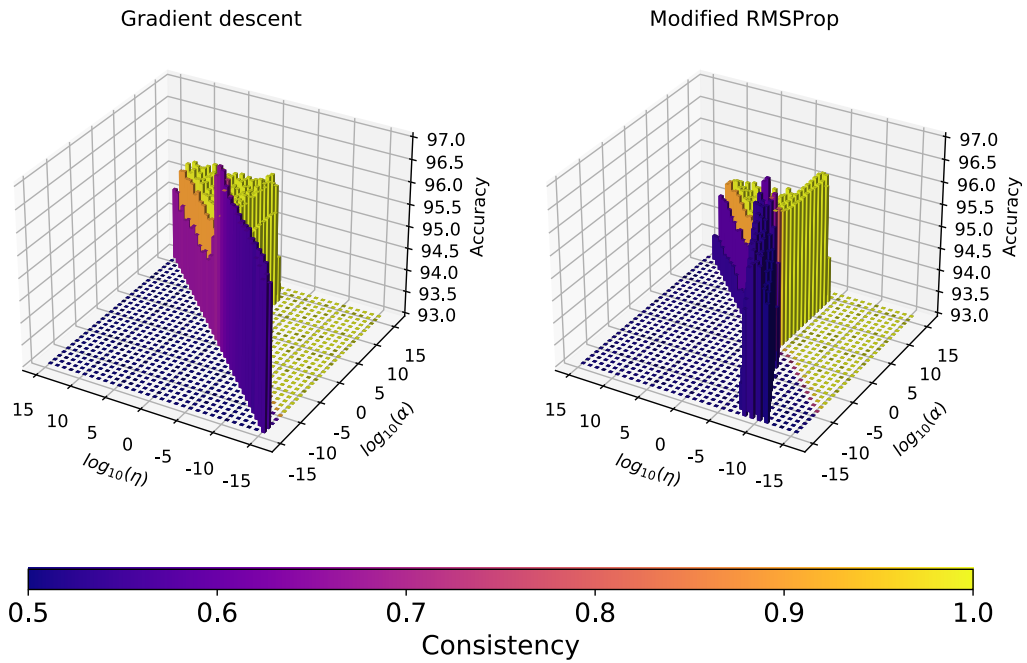


Figure 9. Three dimensional plot that combines Figure 4 and 8. The color represents the consistency of the hidden feature signs shown in Figure 8, and the height of the bar represents the classification accuracy shown in Figure 4. The vertical and horizontal axis represent the logarithmically scaled learning rate  $\eta$  and the scaling factor  $\alpha$ , as in Figures 4 and 8. We can see that the accuracy is high in the region where the learning rate and scaling factor are both small. Additionally, the sign consistency of hidden features is small in these regions, indicating that the learning is not lazy rather has an active behavior.

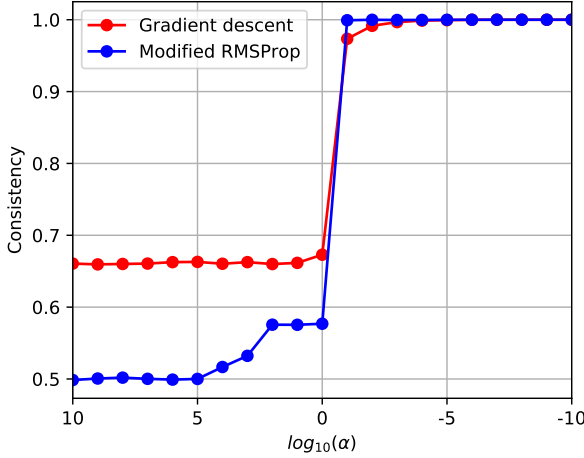


Figure 10. Consistency of the hidden feature signs. The learning rate is picked to have the highest prediction performance for each  $\alpha$ . Therefore, it should be noted that the value of the learning rate is different for each  $\alpha$ . Hidden features are extracted by use of the evaluation dataset of the MNIST.

the training behavior is not lazy, but has an active behavior. From a practical point of view, our observation suggests that, although  $\alpha$  is generally not searched, it is worthwhile to adjust  $\alpha$  as one of the parameters in the hyper-parameter search.

A careful comparison of the regions with small  $\eta$  and  $\alpha$  shows that a difference exists between simple gradient descent and the modified RMSProp. Figure 10 shows that the consistency of the hidden feature signs is different when the high-performing hyper-parameters are used. In the region where a small  $\alpha$  is used, the change from the initial value is larger when an adaptive learning rate optimizer is used. It means that features are likely to be extracted actively, which may be important when building machine learning models with high interpretability such as the attention mechanism (Vaswani et al., 2017). From a different perspective, when models are trained from pre-trained initial parameters, the pre-training impact is likely to be suppressed with an adaptive learning rate optimizer.

## 5. Related Work

From the viewpoint of the implications for the deep learning theory, it is important to note that even in previous studies that did not use an adaptive learning rate, the numerical experiments' interpretation can change significantly with different settings of  $\eta$ . Some previous studies (Chizat et al., 2019; Geiger et al., 2020b; D'Ascoli et al., 2020) check the performance dependency on  $\alpha$  with single  $\eta$  setting. For example, Chizat et al. (2019) reports that the performance with  $\alpha$  just close to the training diverges is the highest, and a

sharp performance decrease as  $\alpha$  increases. Such a behavior can be reproduced by observing slices at  $\eta \sim 10^{-5}$  in our experiment (the gradient descent case in Figures 4, 5, and 6). However, such a sharp drop is not observed at larger  $\eta$ . It is not desirable to have a situation where theoretical research implications can change drastically with just a small setting change. Ideally, it would be possible to experiment numerically with a continuous gradient flow rather than a gradient method of accumulating discrete steps, but that technique has not been established yet. It may be worthwhile to deepen this direction (Geiger et al., 2020b).

One possible reason of a good performance observed near the boundary of the training divergence observed in Chizat et al. (2019) and Figures 4, 5, and 6 is the existence of the so called *Catapult phase*. Lewkowycz et al. (2020) showed there are three training dynamics (*Lazy phase*, *Catapult phase*, *Divergent phase*) based on the learning rate setting. Observed good performance and learning rate configuration looks consistent to the behavior of the *Catapult phase*. For the modified RMSProp, although the training has not diverged numerically like in the simple gradient descent cases, a similar trend has been observed.

## 6. Conclusion

In this paper, we have shown that when output scale change and an adaptive learning rate optimizer are used simultaneously in training of a neural network, the effective learning rate unintentionally depends on the scaling factor  $\alpha$ . Such behavior can lead to the misinterpretation of experimental results. Therefore, we have proposed an optimizer for canceling the dependency of the  $\alpha$  on the effective learning rate. Using the modified optimizer, we have succeeded in comparing the changes in behavior with and without adaptive learning rate for the first time. We have observed some interesting phenomenon, especially with  $\alpha < 1.0$ , such as changes in robustness, proper hyper-parameter setting, and hidden feature consistency during the training.

## References

- Allen-Zhu, Z., Li, Y., and Song, Z. A Convergence Theory for Deep Learning via Over-Parameterization. volume 97 of *Proceedings of Machine Learning Research*, pp. 242–252, 2019.
- Arora, S., Du, S., Hu, W., Li, Z., and Wang, R. Fine-Grained Analysis of Optimization and Generalization for Overparameterized Two-Layer Neural Networks. volume 97 of *Proceedings of Machine Learning Research*, pp. 322–332, 2019.
- Arora, S., Du, S. S., Li, Z., Salakhutdinov, R., Wang, R., and Yu, D. Harnessing the Power of Infinitely Wide Deep

Nets on Small-data Tasks. In *International Conference on Learning Representations*, 2020.

Bai, Y. and Lee, J. D. Beyond Linearization: On Quadratic and Higher-Order Approximation of Wide Neural Networks. In *International Conference on Learning Representations*, 2020.

Chizat, L. and Bach, F. On the Global Convergence of Gradient Descent for Over-parameterized Models using Optimal Transport. In *Advances in Neural Information Processing Systems*, volume 31, pp. 3036–3046, 2018.

Chizat, L. and Bach, F. Implicit Bias of Gradient Descent for Wide Two-layer Neural Networks Trained with the Logistic Loss. In *Proceedings of Thirty Third Conference on Learning Theory*, volume 125 of *Proceedings of Machine Learning Research*, pp. 1305–1338, 2020.

Chizat, L., Oyallon, E., and Bach, F. On Lazy Training in Differentiable Programming. In *Advances in Neural Information Processing Systems* 32, pp. 2937–2947. 2019.

D’Ascoli, S., Refinetti, M., Biroli, G., and Krzakala, F. Double Trouble in Double Descent: Bias and Variance(s) in the Lazy Regime. In *Proceedings of the 37th International Conference on Machine Learning*, volume 119, pp. 2280–2290, 2020.

Du, S. S., Hou, K., Salakhutdinov, R. R., Poczos, B., Wang, R., and Xu, K. Graph Neural Tangent Kernel: Fusing Graph Neural Networks with Graph Kernels. In *Advances in Neural Information Processing Systems* 32, pp. 5723–5733. 2019a.

Du, S. S., Zhai, X., Poczos, B., and Singh, A. Gradient Descent Provably Optimizes Over-parameterized Neural Networks. In *International Conference on Learning Representations*, 2019b.

Geiger, M., Jacot, A., Spigler, S., Gabriel, F., Sagun, L., d’Ascoli, S., Biroli, G., Hongler, C., and Wyart, M. Scaling description of generalization with number of parameters in deep learning. *Journal of Statistical Mechanics: Theory and Experiment*, 2020(2):023401, 2020a.

Geiger, M., Spigler, S., Jacot, A., and Wyart, M. Disentangling feature and lazy training in deep neural networks. *Journal of Statistical Mechanics: Theory and Experiment*, 2020(11):113301, 2020b.

Ghorbani, B., Mei, S., Misiakiewicz, T., and Montanari, A. Limitations of Lazy Training of Two-layers Neural Network. In *Advances in Neural Information Processing Systems*, volume 32, pp. 9111–9121, 2019.

He, K., Zhang, X., Ren, S., and Sun, J. Deep Residual Learning for Image Recognition. In *Proceedings of the IEEE Conference on Computer Vision and Pattern Recognition*, 2016.

Jacot, A., Gabriel, F., and Hongler, C. Neural Tangent Kernel: Convergence and Generalization in Neural Networks. In Bengio, S., Wallach, H., Larochelle, H., Grauman, K., Cesa-Bianchi, N., and Garnett, R. (eds.), *Advances in Neural Information Processing Systems 31*, pp. 8571–8580. 2018.

Kingma, D. P. and Ba, J. Adam: A method for stochastic optimization. In *International Conference on Learning Representations*, 2015.

Krizhevsky, A., Nair, V., and Hinton, G. CIFAR-10 (Canadian Institute for Advanced Research).

LeCun, Y. and Cortes, C. MNIST handwritten digit database. 2010.

LeCun, Y., Simard, P. Y., and Pearlmutter, B. Automatic Learning Rate Maximization by On-Line Estimation of the Hessian’s Eigenvectors. In *Advances in Neural Information Processing Systems* 5, pp. 156–163. 1993.

LeCun, Y., Bottou, L., Orr, G., and Muller, K. "Efficient BackProp". In *Neural Networks: Tricks of the trade*, 1998.

LeCun, Y., Bengio, Y., and Hinton, G. Deep Learning. *Nature*, 521(7553):436–444, 2015.

Lee, J., Xiao, L., Schoenholz, S., Bahri, Y., Novak, R., Sohl-Dickstein, J., and Pennington, J. Wide Neural Networks of Any Depth Evolve as Linear Models Under Gradient Descent. In *Advances in Neural Information Processing Systems* 32, pp. 8572–8583. 2019.

Lee, J., Schoenholz, S., Pennington, J., Adlam, B., Xiao, L., Novak, R., and Sohl-Dickstein, J. Finite Versus Infinite Neural Networks: an Empirical Study. *ArXiv*, abs/2007.15801, 2020.

Lewkowycz, A., Bahri, Y., Dyer, E., Sohl-Dickstein, J., and Gur-Ari, G. The large learning rate phase of deep learning: the catapult mechanism. *ArXiv*, abs/2003.02218, 2020.

Li, Y., Ma, T., and Zhang, H. R. Learning Over-Parametrized Two-Layer Neural Networks beyond NTK. volume 125 of *Proceedings of Machine Learning Research*, pp. 2613–2682, 2020.

Mei, S., Montanari, A., and Nguyen, P.-M. A mean field view of the landscape of two-layer neural networks. *Proceedings of the National Academy of Sciences*, 115(33): E7665–E7671, 2018.

Simonyan, K. and Zisserman, A. Very Deep Convolutional Networks for Large-Scale Image Recognition. In *International Conference on Learning Representations*, 2015.

Tieleman, T. and Hinton, G. Lecture 6.5—RMSProp: Divide the gradient by a running average of its recent magnitude. COURSERA: Neural Networks for Machine Learning, 2012.

Vaswani, A., Shazeer, N., Parmar, N., Uszkoreit, J., Jones, L., Gomez, A. N., Kaiser, L. u., and Polosukhin, I. Attention is All you Need. In *Advances in Neural Information Processing Systems*, volume 30, pp. 5998–6008, 2017.

Woodworth, B., Gunasekar, S., Lee, J. D., Moroshko, E., Savarese, P., Golan, I., Soudry, D., and Srebro, N. Kernel and Rich Regimes in Overparametrized Models. volume 125 of *Proceedings of Machine Learning Research*, pp. 3635–3673, 2020.

Xiao, H., Rasul, K., and Vollgraf, R. Fashion-MNIST: a Novel Image Dataset for Benchmarking Machine Learning Algorithms, 2017.

## A. Performances on training dataset

In addition to the performance for evaluation dataset shown in Figures 4, 5 and 6, we provide the performance for training dataset in Figures 11, 12 and 13.

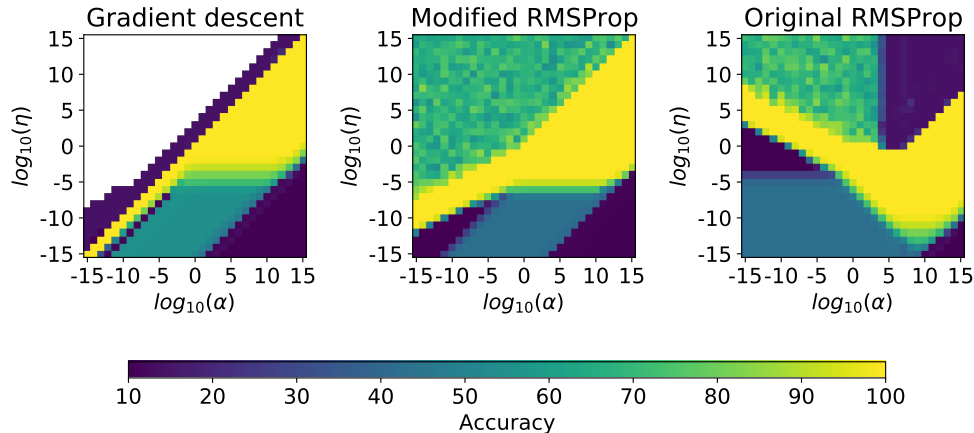


Figure 11. Two-dimensional plots of classification accuracy on the MNIST training dataset. The white area in the figure of gradient descent represents the divergence of training errors.

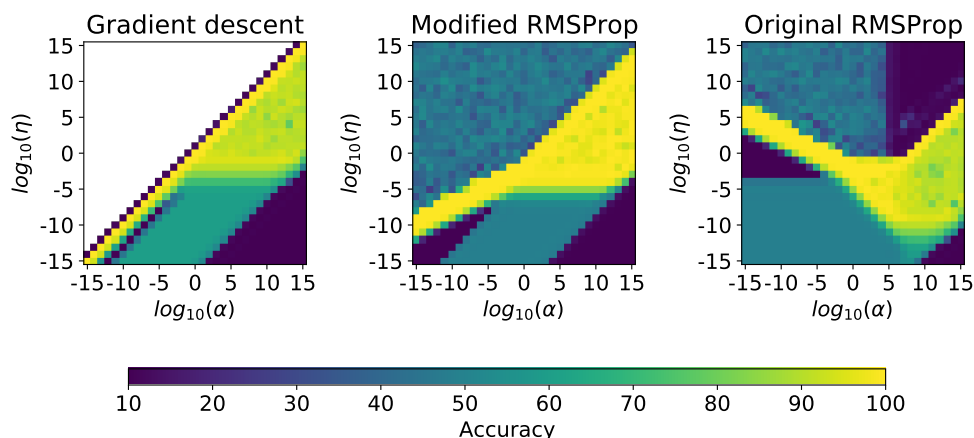


Figure 12. Two-dimensional plots of classification accuracy on the Fashion-MNIST training dataset. The white area in the figure of gradient descent represents the divergence of training errors.

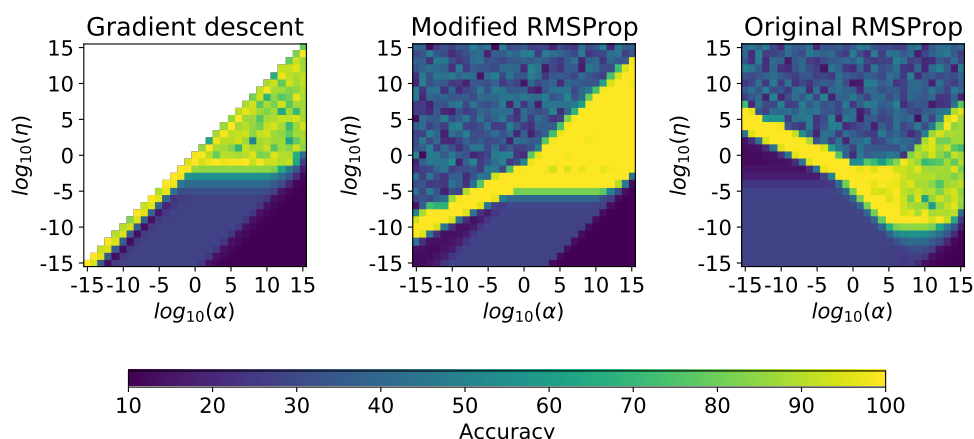


Figure 13. Two-dimensional plots of classification accuracy on the CIFAR-10 training dataset. The white area in the figure of gradient descent represents the divergence of training errors.